

Mixing It Up: Exploring Mixer Networks for Irregular Multivariate Time Series Forecasting

Christian Klöttergens^{1,2}, Vijaya Krishna Yalavarthi^{1,2}, Tim Dornedde¹,
Lars Schmidt-Thieme^{1,2}

¹University of Hildesheim, Information Science and Machine Learning Lab (ISMLL)

²VFWS Data Analytics Research Center

Abstract

Forecasting irregularly sampled multivariate time series with missing values (IMTS) is a fundamental challenge in domains such as healthcare, climate science, and biology. While recent advances in vision and time series forecasting have shown that lightweight MLP-based architectures (e.g., MLP-Mixer, TSMixer) can rival attention-based models in both accuracy and efficiency, their applicability to irregular and sparse time series remains unexplored. In this paper, we propose **IMTS-Mixer**, a novel architecture that adapts the principles of Mixer models to the IMTS setting. IMTS-Mixer introduces two key components: (1) **ISCAM**, a channel-wise encoder that transforms irregular observations into fixed-size vectors using simple MLPs, and (2) **ConTP**, a continuous time decoder that supports forecasting at arbitrary time points. We evaluate IMTS-Mixer on two challenging IMTS benchmarks—PMAU and Physiome-ODE—covering a total of 54 datasets. Our model achieves state-of-the-art performance in both forecasting accuracy and inference time, while using significantly fewer parameters than existing baselines.

Code — <https://anonymous.4open.science/r/IMTS-Mixer-682E>

1 Introduction

Time series forecasting is a critical task across various domains. While a significant body of research has focused on forecasting regularly sampled, fully observed multivariate time series, many real-world applications, such as healthcare, economics, astronomy, and climate, deal with time series data that are *irregularly* sampled, with observations missing across different channels and timestamps. When such data are aligned to a global timeline, the result is a highly sparse and uneven multivariate structure, as illustrated in Figure 1. We refer to such data as **irregularly sampled multivariate time series with missing values (IMTS)**.

Traditional approaches to modeling IMTS have relied on Neural-ODE frameworks, where the time series is modeled as the solution to an ordinary differential equation with a neural network-defined vector field (Rubanova, Chen, and Duvenaud 2019; De Brouwer et al. 2019; Schirmer et al. 2022). While powerful in principle, these models tend to be computationally expensive due to the sequential nature of ODE solvers, and they lack a systematic way to handle missing values.

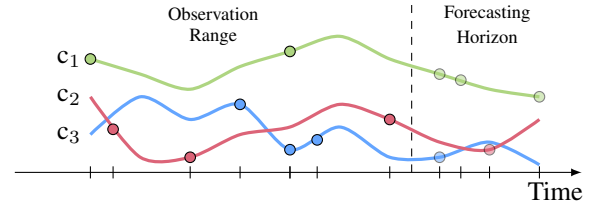


Figure 1: Example of an IMTS Forecasting task. The observations and forecasting targets are irregularly spaced.

Recently, attention-based models have emerged as a more efficient and accurate alternative, achieving competitive performance on IMTS forecasting tasks (Yalavarthi et al. 2024a; Zhang et al. 2024a; Liu, Cao, and Chen 2025). These models typically transform irregular channel-wise observations into fixed-size representations and apply attention mechanisms to capture inter- and intra-channel dependencies. However, such models are often resource-intensive, requiring a large number of parameters and high memory requirements.

Inspired by advances in computer vision, particularly the success of the MLP-Mixer architecture, recent work has demonstrated that carefully arranged MLP-based models can rival or even surpass attention-based models (Tolstikhin et al. 2021). This insight has also been applied to forecasting tasks with regularly sampled time series (Ekambaram et al. 2023; Chen et al. 2023). However, this line of research has not yet been extended to irregularly sampled time series with missing values.

In this paper, we introduce **IMTS-Mixer**, a novel architecture for forecasting with IMTS that combines the simplicity of MLP-based designs with specialized modules to address irregular sampling and forecasting at arbitrary time points. First, we propose the **Irregularly Sampled Channel Aggregation Module (ISCAM)**, a lightweight encoder that maps each irregular channel into a fixed-size representation using simple MLPs. These embeddings are then concatenated and processed by an MLP-Mixer-style architecture to learn inter- and intra-channel interactions. Second, to support continuous-time forecasting, we introduce the **Continuous Temporal Projection (ConTP)** module, a decoder that takes the mixer output, a continuous-valued target

PMAU (ICML '24)				
	Avg. Rank	%Gap-MSE	#Params.	Inf. Time
GraFITi	2	2.9%	313k	2.2s
tPATCHGNN	2.75	5.2%	265k	4.2s
TimeCHEAT	9.75	31%	751k	46s
IMTS-Mixer	1.25	1.3%	204k	1.3s

Physiome-ODE (ICLR '25)				
	Avg. Rank	%Gap-MSE	#Params.	Inf. Time
GraFITi	3.20	42%	883k	0.32s
tPATCHGNN	5.94	79%	287k	0.14s
TimeCHEAT	5.86	141%	566k	2.5s
IMTS-Mixer	1.20	4.1%	136k	0.07s

Table 1: Aggregated results for selected models on two benchmarks: PMAU (Zhang et al. 2024a) and Physiome-ODE (Klöttergens et al. 2024). We report the average ranks by MSE test error (**Avg. Rank**) and the average %-Gap to the best performing model (**%Gap-MSE**). Additionally, we show the average number of parameters (**#Params.**) and inference time for the complete test set of each sub-task (**Inf. Time**). For all metrics, lower is better.

timestamp, and a channel identifier to generate a prediction.

In an extensive comparison, we evaluate IMTS-Mixer on two comprehensive benchmarks:

1. **PMAU** (Zhang et al. 2024a), consisting of four IMTS datasets (Physionet 2012, MIMIC-III, Activity, and USHCN).
2. **Physiome-ODE** (Klöttergens et al. 2024), a benchmark of 50 IMTS datasets derived from biological ODE models.

As shown in Section 1, IMTS-Mixer achieves state-of-the-art forecasting performance, ranking first across both benchmarks.

Our contributions are summarized as follows:

- We propose **IMTS-Mixer**, a novel MLP-based architecture tailored for irregularly sampled multivariate time series with missing values (IMTS), combining efficient channel aggregation and continuous-time prediction.
- We introduce **ISCAM**, a simple and effective channel-wise encoder that maps irregularly observed channels to fixed-size representations, enabling MLP processing.
- We develop a lightweight temporal projection module (**ConTP**) that maps a fixed-size representation of an input channel to future IMTS predictions.
- We conduct extensive experiments on two challenging IMTS benchmarks—PMAU and Physiome-ODE—covering a total of **54 datasets**—and demonstrate that IMTS-Mixer outperforms state-of-the-art models in both forecasting accuracy and computational efficiency.

2 Related Work

2.1 Regular Multivariate Forecasting

The Regular Multivariate Time Series forecasting literature recently focused on transformer-based (Vaswani et al. 2017)

architectures (Zhou et al. 2021; Wu et al. 2021; Zhou et al. 2022; Nie et al. 2022; Liu et al. 2023). However, Zeng et al. showed that a simple model based on linear layers (DLin-ear (Zeng et al. 2023)) can be competitive and partially outperform some of the more complex transformer architectures. Additionally, mixer architectures have been adapted from the computer vision domain (Tolstikhin et al. 2021) to time series (Ekambaram et al. 2023; Chen et al. 2023). They exclusively rely on fully-connected networks that are alternately applied along the channel and time dimension and achieve state-of-the-art results.

2.2 IMTS Forecasting

Initially, researchers relied on Neural ODE-based (Chen et al. 2018) approaches to model IMTS (Rubanova, Chen, and Duvenaud 2019; De Brouwer et al. 2019; Biloš et al. 2021; Schirmer et al. 2022). ODEs are the prevalent framework in science and engineering to model how systems evolve over time in a continuous manner. However, using neural networks to represent ODE systems has proven to be less effective than other IMTS modeling approaches and also incurs relatively long inference times (Yalavarthi et al. 2024a; Zhang et al. 2024a).

Graph Transformers for IMTS forecasting. Apart from the ODE-based approaches the Transformable Patch Graph Neural Network (tPatchGNN) (Zhang et al. 2024a) applies a patching mechanism to each channel. The patches are then processed with a Transformer and serve as input for a Graph Neural Network (GNN) that models inter-channel dependencies. Additionally, we want to highlight Graphs for Forecasting Irregular Multivariate Time Series (GraFITi) (Yalavarthi et al. 2024a). Here, the IMTS is represented with a graph in which channels and time steps are nodes and observed values are stored in the edges between the corresponding time and channel nodes. Forecasts are made by predicting the edge values of query-time nodes with graph attention layers. While this approach provides state-of-the-art performance, it also comes with major drawbacks that relate to the graph structure itself. GraFITi relies on time nodes that are connected to multiple channel nodes, corresponding to observation steps that observe more than one channel. If only one channel is observed at a time, the resulting graph is disconnected, rendering GraFITi incapable of modeling inter-channel interactions. Another problem of GraFITi lies in the fact that the query nodes are indirectly connected and hence influence each other. This entails that predictions will change depending on what *other* queries we give to the model.

TimeCHEAT (Liu, Cao, and Chen 2025) transforms an IMTS into regularly observed patches using a GraFITi-based encoder. These patches are then further processed by a transformer and a linear decoder to obtain the final predictions.

3 Mixer Networks

MLP-Mixer. The MLP-Mixer (Tolstikhin et al. 2021) was originally proposed as a simple and efficient alternative to convolutional neural networks (CNNs) and Vision Transformers (ViTs) for image classification tasks. In this archi-

texture, a 2D image ($\in \mathbb{R}^{W \times H}$) where W, H are width and height) is divided into P non-overlapping patches, which are flattened and projected into vectors of length C , resulting in an input representation $X \in \mathbb{R}^{P \times C}$.

The core of the MLP-Mixer consists of a stack of mixer layers, each containing two separate MLP blocks:

- a **token-mixing MLP** $\text{MLP}_P : \mathbb{R}^P \rightarrow \mathbb{R}^P$ operating across patches (rows of X),
- a **channel-mixing MLP** $\text{MLP}_C : \mathbb{R}^C \rightarrow \mathbb{R}^C$ operating across channels (columns of X).

Each MLP block is preceded by layer normalization and followed by a residual connection. Formally, given input $X \in \mathbb{R}^{P \times C}$, the output of a single mixer layer is computed as:

$$U_{*,c} = X_{*,c} + \text{LayerNorm}(\text{MLP}_C(X_{*,c})), \quad c = 1, \dots, C$$

$$Z_{p,*} = U_{p,*} + \text{LayerNorm}(\text{MLP}_P(U_{p,*})), \quad p = 1, \dots, P$$

Here, $X_{*,c}$ denotes the c -th column (channel vector), and $X_{p,*}$ denotes the p -th row (patch vector).

Despite its simplicity and lack of attention mechanisms, MLP-Mixer has demonstrated competitive performance, often outperforming more complex models such as Vision Transformers (Dosovitskiy et al. 2020) on various image classification benchmarks.

TSMixer. Motivated by the success of MLP-Mixer in vision, Chen et al. (2023) proposed *TSMixer*, an adaptation of the Mixer architecture for regular multivariate time series forecasting. The goal is to predict the next Q time steps $Y \in \mathbb{R}^{Q \times C}$ from a past window of T time steps $X \in \mathbb{R}^{T \times C}$, where C denotes the number of variables (channels).

TSMixer applies a stack of Mixer layers to the input X , where:

- The **temporal mixer** (analogous to token-mixing in images) mixes information across time steps:
 $\text{MLP}_T : \mathbb{R}^T \rightarrow \mathbb{R}^T$,
- The **channel mixer** operates across variables:
 $\text{MLP}_C : \mathbb{R}^C \rightarrow \mathbb{R}^C$.

Similar to MLP-Mixer, these mixers are applied alternately with residual connections and layer normalization. After the stack of mixer layers, a final linear projection $\mathbb{R}^T \rightarrow \mathbb{R}^Q$ is applied across the temporal axis to produce the forecast $Y \in \mathbb{R}^{Q \times C}$.

4 The IMTS Forecasting Problem

Irregularly Sampled Multivariate Time Series (IMTS). Following Shukla and Marlin (2020), we define an *irregularly sampled multivariate time series (IMTS)* as a collection of C unaligned, sparse, and independently sampled univariate time series, one per channel:

$$X := [X_1, \dots, X_C] \in \mathcal{X}$$

where each channel $X_c \in \text{Seq}(\mathbb{R} \times \mathbb{R})$ is a sequence of observation tuples

$$X_c := ((t_{c,i}, v_{c,i}))_{i=1}^{N_c}$$

with $t_{c,i} \in \mathbb{R}$: the timestamp of the i -th observation in channel c and $v_{c,i} \in \mathbb{R}$: the observed value at time $t_{c,i}$. Channels may be observed at different timestamps and with different sequence lengths N_c , resulting in irregular and sparse structure when aligned over a global timeline.

Forecasting Query. Analogous to the IMTS definition, we define a *forecasting query* as a collection of per-channel timepoints at which future values should be predicted:

$$Q := [Q_1, \dots, Q_C] \in \mathcal{Q}, \quad \text{where}$$

$$Q_c = (q_{c,i})_{i=1}^{K_c} \in \text{Seq}(\mathbb{R})$$

Each $q_{c,i}$ specifies a future timestamp for which a value prediction is required for channel c . The corresponding **forecasting answer** is given by:

$$Y := [Y_1, \dots, Y_C] \in \mathcal{Y}, \quad \text{where}$$

$$Y_c = (y_{c,i})_{i=1}^{K_c} \in \text{Seq}(\mathbb{R})$$

ensuring $|Q_c| = |Y_c| = K_c$ for each channel c .

Problem 1 IMTS Forecasting Problem. Given a training dataset of M triples: $\{(X^{(m)}, Q^{(m)}, Y^{(m)})\}_{m=1}^M$ drawn from an unknown distribution ρ over $\mathcal{X} \times \mathcal{Q} \times \mathcal{Y}$, and a loss function $\ell : \mathcal{Y} \times \mathcal{Y} \rightarrow \mathbb{R}$ (e.g., mean squared error), the goal is to learn a model: $\hat{Y} : \mathcal{X} \times \mathcal{Q} \rightarrow \mathcal{Y}$ that minimizes the expected loss:

$$\mathcal{L}(\hat{Y}; \rho) := \mathbb{E}_{(X, Q, Y) \sim \rho} [\ell(Y, \hat{Y}(X, Q))] \quad (1)$$

5 IMTS-Mixer

Each IMTS consists of C channels, where the number of observations N_c for each channel c may vary, both within a single IMTS and across different samples. This irregularity makes it challenging to directly apply standard neural architectures, particularly MLP-Mixers, which require fixed-size input representations.

To address this, we propose the **Irregularly Sampled Channel Aggregation Module (ISCAM)**, which encodes each variable-length channel X_c into a fixed-dimensional vector $Z_c \in \mathbb{R}^D$, enabling uniform downstream processing using MLP-Mixer blocks.

5.1 Irregularly Sampled Channel Aggregation Module

Let a single channel X_c represent a sequence of N_c observations. Our goal is to transform this irregular sequence into a fixed-size embedding $Z_c \in \mathbb{R}^D$. For clarity, we drop the channel subscript c and denote the observations as (t_i, v_i) .

Observation-Tuple Embedding. Each observation tuple (t_i, v_i) is embedded using a shared MLP $f_{\text{OTE}} : \mathbb{R}^2 \rightarrow \mathbb{R}^D$, resulting in:

$$H = [h_1, \dots, h_{N_c}] \in \mathbb{R}^{N_c \times D}, \quad \text{where } h_i = f_{\text{OTE}}([v_i, t_i])$$

Weighted Aggregation. To compute an importance score for each observation, we apply a second shared MLP $f_{\text{WA}} : \mathbb{R}^2 \rightarrow \mathbb{R}^D$:

$$A = [a_1, \dots, a_{N_c}] \in \mathbb{R}^{N_c \times D}, \quad \text{where } a_i = f_{\text{WA}}([v_i, t_i])$$

Unlike standard attention mechanisms which compute a scalar weight per observation, we assign a separate weight to each embedding feature, similar to multi-head attention, but without cross-token interactions.

To handle the variable length N_c across samples and ensure scale invariance, we apply softmax normalization along the columns d :

$$\text{softmax} : \mathbb{R}^{N_c} \rightarrow \mathbb{R}^{N_c}, \quad \text{so that } \sum_{i=1}^{N_c} \text{softmax}(a_{i,d}) = 1$$

Let $A_{:,d} = (a_{1,d}, \dots, a_{N_c,d})$ and $H_{:,d} = (h_{1,d}, \dots, h_{N_c,d})$ denote the d -th column across the N_c elements of A and H , respectively. The final channel embedding is then computed as:

$$Z_c = \left[\sum_{i=1}^{N_c} \text{softmax}(A_{:,d})_i \cdot H_{:,d} \right]_{d=1}^D \in \mathbb{R}^D \quad (2)$$

This yields a fixed-size vector per channel, where each dimension is an importance-weighted average over time.

While one can have channel-specific parameters in f_{OTE} and f_{WA} we allow to share the parameters to reduce the number of parameters.

Channel Bias. Since the embedding MLPs are shared across all channels, global channel-specific information may be lost. To address this, we introduce a *channel bias* vector $b_c \in \mathbb{R}^D$ for each channel c , composed of learnable parameters. The final channel encoding is computed as:

$$Z_c^+ = Z_c + b_c \in \mathbb{R}^D \quad (3)$$

This allows the model to retain per-channel identity and compensate for missing patterns or context. In the case where a channel c is missing (i.e., X_c is empty), we define $Z_c := 0$ so that the output $Z_c^+ = b_c$ contains only the bias information.

Comparison with Existing Architectures. Several prior models such as SeFT (Horn et al. 2020), Tripletformer (Yalavarthi, Burchert, and Schmidt-Thieme 2023), and GraFITi (Yalavarthi et al. 2024a) use attention-based mechanisms over IMTS observations, where the aggregation is performed via a softmax-weighted sum of encoded tuples. These methods compute weights through the scaled dot-product of learned queries and keys, following the standard attention framework (Vaswani et al. 2017).

In contrast, ISCAM bypasses query-key interactions entirely by modeling importance weights directly through a learned MLP applied to each observation tuple. This results in a simpler and more lightweight design, while still enabling dimension-specific weighting through softmax normalization.

TTCN (Zhang et al. 2024a,b) also employs MLP-based aggregation over irregular time series. However, it introduces a more complex mechanism by using separate MLPs

(called filters) for each embedding dimension d . Moreover, TTCN lacks a dedicated channel bias component, which limits its ability to encode global per-channel information independent of input observations.

Empirically, we show that ISCAM serves as a more effective embedding module compared to multi-head attention and TTCN in Table 5, particularly when paired with MLP-Mixer architectures for IMTS forecasting.

5.2 Mixer Blocks

Similar to MLP-Mixer and TSMixer, we employ L mixer blocks, each operating over the channel and feature dimensions. A single mixer block at layer l updates the representation $Z^{(l-1)} \in \mathbb{R}^{C \times D}$ as follows:

$$\begin{aligned} Z'^{(l)} &= Z^{(l-1)} + \text{ReLU} \left(\text{Linear}_{\text{CHAN}}^{(l)} \left(\text{RMS}(Z^{(l-1)\top}) \right) \right)^\top \\ Z^{(l)} &= Z^{(l-1)} + Z'^{(l)} + \text{ReLU} \left(\text{Linear}_{\text{DIM}}^{(l)} \left(\text{RMS}(Z'^{(l)}) \right) \right) \end{aligned} \quad (4)$$

Here, $\text{Linear}_{\text{CHAN}}^{(l)}$ operates along the channel dimension (i.e., across C channels), $\text{Linear}_{\text{DIM}}^{(l)}$ operates along the feature dimension (D), RMS denotes RMSNorm (Zhang and Sennrich 2019), and ReLU is the element-wise nonlinearity.

Compared to MLP-Mixer and TSMixer described in Section 3, we introduce two modifications to adapt to the irregular multivariate forecasting setting:

- **Flexible Output Dimension:** We allow the output of the final mixer layer to have a configurable feature dimension D_{OUT} , i.e., $Z^{(L)} \in \mathbb{R}^{C \times D_{\text{OUT}}}$. This makes it possible to match the projection to varying numbers of queries per channel. All intermediate layers maintain a fixed hidden size D .
- **RMSNorm Instead of LayerNorm:** We replace LayerNorm with RMSNorm (Zhang and Sennrich 2019), which has been shown to yield faster convergence while maintaining predictive performance.

5.3 Continuous Temporal Projection

TSMixer utilizes a linear layer to project the encoded representation of each channel to forecasts on a predefined regular grid of query steps (Chen et al. 2023). This design, however, is incompatible with IMTS, where query times are not fixed but vary continuously across instances.

To address this, IMTS-Mixer introduces a **Continuous Temporal Projection (ConTP)**, which allows the model to project the hidden state of each channel to any given point in time. Instead of learning linear layers tied to predetermined query steps, ConTP learns a function $f_{\text{QU}} : \mathbb{R} \rightarrow \mathbb{R}^{D_{\text{OUT}}}$ that maps scalar query times to the weights of a linear projection dynamically. Formally, the forecast for channel c at query time $q_{c,i}$ is computed as:

$$\hat{y}_{i,c} = f_{\text{QU}}^c(q_{c,i}) \cdot Z_c^{(L)} + b_c^{\text{OUT}} \in \mathbb{R} \quad (5)$$

In order to enhance expressiveness, we learn a separate function f_{QU}^c for each channel and implement this with a two-layer MLP.

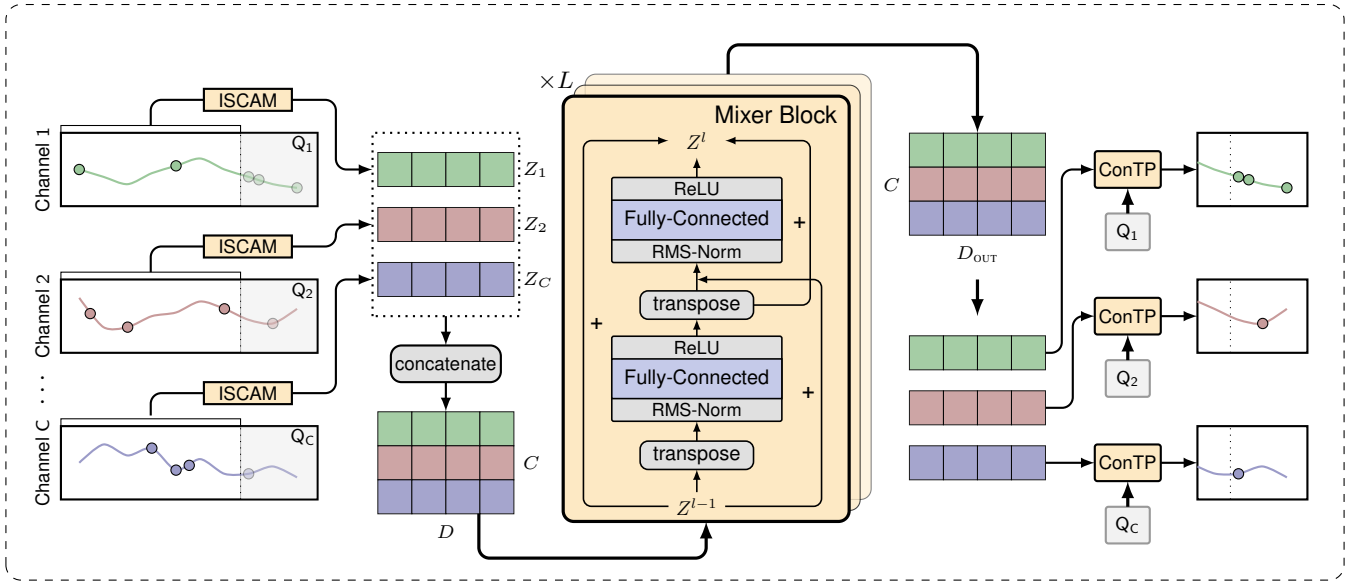


Figure 2: Overview of IMTS-Mixer’s architecture

Additionally, we learn a query independent output bias $b^{\text{out}} \in \mathbb{R}^C$.

The complete architecture of IMTS-Mixer is illustrated in Figure 2.

6 Experiments

We evaluate IMTS-Mixer on two benchmarks: First, we compare on the PMAU benchmark as introduced by Zhang et al. (Zhang et al. 2024a). This benchmark, contains the four datasets **PhysioNet** (Silva et al. 2012), **MIMIC** (Johnson et al. 2016) **Human Activity** (Vedrana Vidulin 2010) and **USHCN** (Menne, Williams, and Vose 2006) and we provide a more detailed description of each dataset in the appendix. Second, we use the recently published **Physiome-ODE** benchmark (Klöttergens et al. 2024) which contains 50 semi-synthetic IMTS datasets generated from Biological ODEs. We refer to the Appendix for detailed information on hyperparameters.

6.1 PMAU

The baseline models already established in the PMAU benchmark originate from regular multivariate time series forecasting, IMTS classification and IMTS forecasting. DLinear (Zeng et al. 2023), TimesNet (Wu et al. 2022), PatchTST (Nie et al. 2022) and Crossformer (Zhang and Yan 2022) are state-of-the-art models for regular multivariate forecasting. These are applied by adding the time stamps and information about missing values as additional channels, which is shown to be an oversimplified and ineffective strategy (Zhang et al. 2024a).

GRU-D (Che et al. 2018), SeFT (Horn et al. 2020), Raindrop (Zhang et al. 2021), Warpformer (Zhang et al. 2023) and mTAND (Shukla and Marlin 2020) are all models primarily introduced for IMTS classification, which are

equipped with a predictor network which inputs hidden IMTS representations and query times.

Finally, Latent-ODE (Rubanova, Chen, and Duvenaud 2019), Continuous Recurrent Units (CRU) (Schirmer et al. 2022), Neural Flow (Biloš et al. 2021), tPatchGNN (Zhang et al. 2024a) and GraFITi (Yalavarthi et al. 2024a) are models designed for IMTS Forecasting. To these baselines we add TimeCHEAT (Liu, Cao, and Chen 2025) and TS-Mixer (Chen et al. 2023) and provide the respective implementation details in Section B.

Table 2 reports the forecasting accuracy of IMTS-Mixer compared to the baseline models. While all models were trained on Mean Squared Error (MSE) we also report the test Mean Absolute Error (MAE). IMTS-Mixer provides the most accurate forecasts on PhysioNet, Human Activity and USHCN for both evaluation metrics MSE and MAE. For MIMIC, our model comes in second, closely behind GraFITi. We observe that GraFITi’s relative performance increases with the number of channels. While it outperforms IMTS-Mixer on MIMIC (102 channels) and is on par with our model on PhysioNet (37 channels), it is significantly outperformed by IMTS-Mixer on Human Activity (12 channels) and USHCN (5 channels).

Additionally, we observe that TimeCHEAT does not provide competitive forecasting accuracy despite being the most recent baseline (AAAI 2025). The model is likely struggling, due to its inability to account for different query time steps. This major flaw is less problematic in very short-term forecasting scenarios, as used in the paper that introduced TimeCHEAT (Liu, Cao, and Chen 2025).

6.2 Physiome-ODE

In order to provide a broader evaluation we compare IMTS-Mixer on the Physiome-ODE benchmark. The 50 datasets, that are contained in Physiome-ODE were created by solv-

	PhysioNet		MIMIC		Human Activity		USHCN	
	MSE $\times 10^{-3}$	MAE $\times 10^{-2}$	MSE $\times 10^{-2}$	MAE $\times 10^{-2}$	MSE $\times 10^{-3}$	MAE $\times 10^{-2}$	MSE $\times 10^{-1}$	MAE $\times 10^{-1}$
TSMixer	8.664 \pm 0.47	4.68 \pm 0.13	1.89 \pm 0.01	7.99 \pm 0.07	3.01 \pm 0.01	3.64 \pm 0.01	5.39 \pm 0.04	3.33 \pm 0.08
DLinear	41.86 \pm 0.05	15.52 \pm 0.03	4.90 \pm 0.00	16.29 \pm 0.05	4.03 \pm 0.01	4.21 \pm 0.01	6.21 \pm 0.00	3.88 \pm 0.02
TimesNet	16.48 \pm 0.11	6.14 \pm 0.03	5.88 \pm 0.08	13.62 \pm 0.07	3.12 \pm 0.01	3.56 \pm 0.02	5.58 \pm 0.05	3.60 \pm 0.04
PatchTST	12.00 \pm 0.23	6.02 \pm 0.14	3.78 \pm 0.03	12.43 \pm 0.10	4.29 \pm 0.14	4.80 \pm 0.09	5.75 \pm 0.01	3.57 \pm 0.02
Crossformer	6.66 \pm 0.11	4.81 \pm 0.11	2.65 \pm 0.10	9.56 \pm 0.29	4.29 \pm 0.20	4.89 \pm 0.17	5.25 \pm 0.04	3.27 \pm 0.09
GRU-D	5.59 \pm 0.09	4.08 \pm 0.05	1.76 \pm 0.03	7.53 \pm 0.09	2.94 \pm 0.05	3.53 \pm 0.06	5.54 \pm 0.38	3.40 \pm 0.28
SeFT	9.22 \pm 0.18	5.40 \pm 0.08	1.87 \pm 0.01	7.84 \pm 0.08	12.20 \pm 0.17	8.43 \pm 0.07	5.80 \pm 0.19	3.70 \pm 0.11
RainDrop	9.82 \pm 0.08	5.57 \pm 0.06	1.99 \pm 0.03	8.27 \pm 0.07	14.92 \pm 0.14	9.45 \pm 0.05	5.78 \pm 0.22	3.67 \pm 0.17
Warpformer	5.94 \pm 0.35	4.21 \pm 0.12	1.73 \pm 0.04	7.58 \pm 0.13	2.79 \pm 0.04	3.39 \pm 0.03	5.25 \pm 0.05	3.23 \pm 0.05
mTAND	6.23 \pm 0.24	4.51 \pm 0.17	1.85 \pm 0.06	7.73 \pm 0.13	3.22 \pm 0.07	3.81 \pm 0.07	5.33 \pm 0.05	3.26 \pm 0.10
Latent-ODE	6.05 \pm 0.57	4.23 \pm 0.26	1.89 \pm 0.19	8.11 \pm 0.52	3.34 \pm 0.11	3.94 \pm 0.12	5.62 \pm 0.03	3.60 \pm 0.12
Neural Flow	7.20 \pm 0.07	4.67 \pm 0.04	1.87 \pm 0.05	8.03 \pm 0.19	4.05 \pm 0.13	4.46 \pm 0.09	5.35 \pm 0.05	3.25 \pm 0.05
CRU	8.56 \pm 0.26	5.16 \pm 0.09	1.97 \pm 0.02	7.93 \pm 0.19	6.97 \pm 0.78	6.30 \pm 0.47	6.09 \pm 0.17	3.54 \pm 0.18
GraFITi	<u>4.89 \pm 0.12</u>	<u>3.65 \pm 0.09</u>	1.53 \pm 0.02	6.68 \pm 0.09	<u>2.65 \pm 0.02</u>	<u>3.09 \pm 0.02</u>	5.17 \pm 0.11	3.22 \pm 0.24
TimeCHEAT	6.18 \pm 0.25	4.40 \pm 0.17	1.76 \pm 0.01	7.67 \pm 0.06	4.42 \pm 0.60	4.90 \pm 0.51	5.70 \pm 0.53	3.51 \pm 0.31
tPatchGNN	4.98 \pm 0.08	3.72 \pm 0.03	1.69 \pm 0.03	7.22 \pm 0.09	2.66 \pm 0.03	3.15 \pm 0.02	<u>5.00 \pm 0.04</u>	<u>3.08 \pm 0.04</u>
IMTS-Mixer	4.88 \pm 0.03	3.46 \pm 0.01	<u>1.61 \pm 0.01</u>	<u>6.83 \pm 0.03</u>	2.50 \pm 0.01	3.05 \pm 0.01	4.91 \pm 0.05	3.02 \pm 0.03

Table 2: Comparison of different algorithms across four datasets based on Test MSE and MAE. We reproduced the results from GraFITi (Yalavarthi et al. 2024a) with the hyperparameters from their GitHub repository (<https://github.com/yalavarthivk/GraFITi>). The results for IMTS-Mixer, TSMixer and TimeCHEAT are from our own experiments. Other results are reported from tPatchGNN (Zhang et al. 2024a). Each training run was repeated 5 times with different random seeds and the standard deviation in between these trials is given after the \pm . We report the best results in **bold** and the second-best results underlined.

	Avg. Rank	# Wins	%Gap-MSE
GraFITi-C	4.70	6	135
Neural Flows	7.68	0	343
CRU	4.44	2	74.4
LinODENet	3.36	<u>7</u>	<u>21.1</u>
GraFITi	<u>3.26</u>	2	41.6
tPatchGNN	4.78	1	79
TimeCHEAT	5.80	1	141
IMTS-Mixer	1.20	42	4.1

Table 3: We report the average rank based on Test MSE, assigning the better rank in case of ties. # Wins indicates the number of datasets where a model achieves the lowest Test MSE. %Gap-MSE refers to the mean relative difference in test MSE compared to the best model on each dataset.

ing Biological ODEs for 100 steps. 80% of the resulting *observations* are dropped uniform at random. Each dataset consists of 2000 IMTS that each have different ODE constants and initial states. We refer to Klötergens et al. (2024) for more details. IMTS-Mixer is compared with GraFITi, LinODENet (Scholz et al. 2022), CRU, Neural Flows and GraFITi-C, a constant variant of GraFITi. Additionally, we add tPatchGNN and TimeCHEAT to the benchmark and refer to Section B for implementation details.

The Physiome-ODE benchmark was originally proposed to highlight the strengths of neural ODEs (Biloš et al. 2021; Schirmer et al. 2022) and in first experiments a member of that model family (LinODENet) had the best forecasting accuracy on most datasets. Now, IMTS-Mixer has the lowest

	PhysioNet	MIMIC	H. Activity	USHCN
GraFITi	251k / 1.9	255k / 4.0	249k / 0.6	496k / 2.2
tPATCHGNN	362k / 2.7	363k / 10	166k / 1.4	167k / 2.5
TimeCHEAT	659k / 33	755k / 72	1262k / 15	330k / 63
IMTS-Mixer	207k / 0.7	497k / 2.9	72k / 0.3	40k / 1.4

Table 4: Number of parameters (left) and inference time (right) in seconds for each dataset of the PMAU benchmark.

test MSE on 42 of 50 datasets, establishing a new state-of-the-art on this benchmark. We list the test MSEs for all 50 datasets in Section C.

6.3 Efficiency Analysis

We conduct our experiments on an NVIDIA 1080Ti with 12 GB of GPU Memory. In Table 4, we compare the inference time and parameter count of recent models to that of IMTS-Mixer. Here, inference time refers to the total time it takes to answer all queries from the test set using a batch size of 32. We observe that IMTS-Mixer’s inference time is consistently shorter than the inference time of competing models. Furthermore, it uses the fewest number of parameters on three out of four datasets. The inference time and number of parameters for the Physiome-ODE datasets are listed in the Section C.

6.4 Evaluating Alternative Components

We conduct an ablation study in which we replace IS-CAM, with Multi-Head Attention (MHA) (Vaswani et al.

	PhysioNet	MIMIC	H. Activity	USHCN
MSE	$\times 10^{-3}$	$\times 10^{-2}$	$\times 10^{-3}$	$\times 10^{-1}$
Encoder				
TTCN	5.07 ± 0.04	1.71 ± 0.05	2.54 ± 0.02	4.94 ± 0.06
MHA	4.94 ± 0.06	1.66 ± 0.01	2.52 ± 0.01	4.94 ± 0.05
ISCAM	4.88 ± 0.03	1.61 ± 0.01	2.50 ± 0.01	4.91 ± 0.05
Temporal Projection				
MLP	4.91 ± 0.03	1.61 ± 0.01	2.51 ± 0.02	5.11 ± 0.03
ConTP	4.88 ± 0.03	1.61 ± 0.01	2.50 ± 0.01	4.91 ± 0.05

Table 5: Comparing Test MSE of IMTS-Mixer variants with different Encoders and Temporal Projection modules.

2017) and Transformable Time-aware Convolution Network (TTCN) (Zhang et al. 2024b). A detailed description on how a MHA is applied in this experiment is given in Section D. The result is shown in Table 5. For a fair comparison, we re-tune the hyperparameters for each IMTS-Mixer modification. Our results show, that among the evaluated candidates ISCAM is the best encoder for our model.

Furthermore, we compare ConTP with using an MLP as temporal projection as implemented in tPatchGNN. Here, a sinusoidal embedding of the query times is concatenated to the hidden state of each channel and the forecast is obtained by a 2-layer MLP that inputs the enriched channel representation and outputs a scalar (Zhang et al. 2024a). On each dataset ConTP shows to be more or equally effective than the existing MLP based method.

6.5 Effect of Mixer Blocks

We conducted an experiment to assess the effect of that the number of mixer layers has on the forecasting accuracy on the four PMAU datasets. The results shown in Figure 3 indicate that having at least one mixer block is necessary to obtain the optimal performance. However, stacking more and more mixer blocks is usually not beneficial on the evaluated datasets. Furthermore, we observe that IMTS-Mixer, without a single mixer block, is already competitive with state-of-the-art baselines, showcasing the ability of ISCAM and ConTP.

7 Limitations

Theoretically, IMTS-Mixer is limited by its fixed-size channel aggregation, which converts the sequence of observations from a channel into a fixed-sized embedding. For very long sequences, or when typical sequence lengths vary significantly across channels, the fixed-size representation may become a bottleneck or fail to adequately capture the diversity across channels. However, in practice, we do not find this to be an issue. Our model is able to fit all the common benchmark datasets well with varying number of channels and distribution of sequence lengths.

Another limitation is that the parameter count in the mixer blocks scales quadratically with the number of channels. We observe that IMTS-Mixer struggles with datasets that contain many channels. On the PMAU benchmark, IMTS-Mixer is outperformed by GraFITi only on the MIMIC

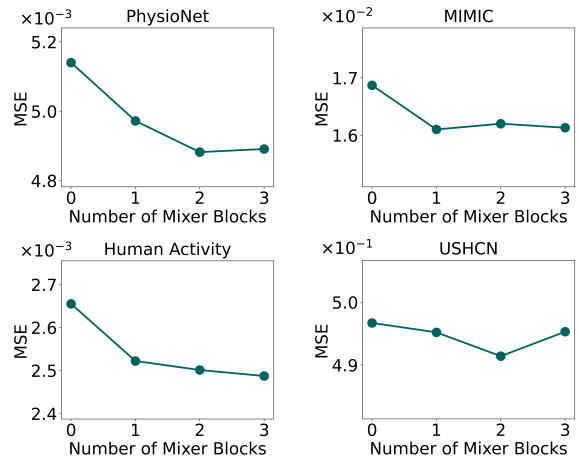


Figure 3: Test MSE with varying number of mixer blocks.

dataset, which has the most channels and is on par with GraFITi on PhysioNet, which has the second-most channels. Furthermore, we find that MIMIC is the only dataset in which IMTS-Mixer does not have the lowest number of parameters, as shown in Table 4. However, on datasets with fewer channels (e.g., Human Activity, USHCN), our model achieves significantly higher forecasting accuracy than competing methods.

8 Conclusion and Future Work

In this work we present IMTS-Mixer, a parameter efficient all MLP-based model for IMTS forecasting. Our architecture incorporates ISCAM, a novel method for aggregating irregularly sampled univariate time series that, despite its simplicity, outperforms existing approaches. Additionally, we generalize linear temporal projection layers to IMTS forecasting targets by introducing ConTP and yield equal or better performance than previously applied solutions.

In our experiments, we show that IMTS-Mixer establishes a new state-of-the-art forecasting accuracy on three real-world and 42 semisynthetic datasets, despite its architectural simplicity. We note that our model has difficulty handling time series with a large number of channels, as the parameter count in the fully connected layers increases significantly, which is associated with higher test error.

For future work, we plan on expanding our model to the related fields of IMTS classification and interpolation. Furthermore, we will investigate IMTS-Mixer’s applicability to probabilistic IMTS forecasting, where it could serve as an encoder of conditional normalizing flows (Yalavarthi et al. 2024b,c).

References

Biloš, M.; Sommer, J.; Rangapuram, S. S.; Januschowski, T.; and Günnemann, S. 2021. Neural Flows: Efficient Alternative to Neural ODEs. In *Advances in Neural Information Processing Systems*, volume 34, 21325–21337. Curran Associates, Inc.

- Che, Z.; Purushotham, S.; Cho, K.; Sontag, D.; and Liu, Y. 2018. Recurrent Neural Networks for Multivariate Time Series with Missing Values. *Scientific Reports*, 8(1): 6085.
- Chen, R. T. Q.; Rubanova, Y.; Bettencourt, J.; and Duvenaud, D. K. 2018. Neural Ordinary Differential Equations. In *Advances in Neural Information Processing Systems*, volume 31. Curran Associates, Inc.
- Chen, S.-A.; Li, C.-L.; Arik, S. O.; Yoder, N. C.; and Pfister, T. 2023. TSMixer: An All-MLP Architecture for Time Series Forecasting. *Transactions on Machine Learning Research*.
- De Brouwer, E.; Simm, J.; Arany, A.; and Moreau, Y. 2019. GRU-ODE-Bayes: Continuous Modeling of Sporadically-Observed Time Series. In *Advances in Neural Information Processing Systems*, volume 32. Curran Associates, Inc.
- Defazio, A.; Yang, X. A.; Mehta, H.; Mishchenko, K.; Khaled, A.; and Cutkosky, A. 2024. The Road Less Scheduled. arXiv:2405.15682.
- Dosovitskiy, A.; Beyer, L.; Kolesnikov, A.; Weissenborn, D.; Zhai, X.; Unterthiner, T.; Dehghani, M.; Minderer, M.; Heigold, G.; Gelly, S.; Uszkoreit, J.; and Houlsby, N. 2020. An Image Is Worth 16x16 Words: Transformers for Image Recognition at Scale. In *International Conference on Learning Representations*.
- Ekambaram, V.; Jati, A.; Nguyen, N.; Sinthong, P.; and Kalagnanam, J. 2023. TSMixer: Lightweight MLP-Mixer Model for Multivariate Time Series Forecasting. In *Proceedings of the 29th ACM SIGKDD Conference on Knowledge Discovery and Data Mining, KDD '23*, 459–469. Association for Computing Machinery. ISBN 9798400701030.
- Horn, M.; Moor, M.; Bock, C.; Rieck, B.; and Borgwardt, K. 2020. Set Functions for Time Series. In *Proceedings of the 37th International Conference on Machine Learning*, 4353–4363. PMLR.
- Johnson, A. E. W.; Pollard, T. J.; Shen, L.; Lehman, L.-w. H.; Feng, M.; Ghassemi, M.; Moody, B.; Szolovits, P.; Anthony Celi, L.; and Mark, R. G. 2016. MIMIC-III, a Freely Accessible Critical Care Database. *Scientific Data*, 3(1): 160035.
- Kingma, D. P.; and Ba, J. 2017. Adam: A Method for Stochastic Optimization. arXiv:1412.6980.
- Klöttergens, C.; Yalavarthi, V. K.; Scholz, R.; Stubbemann, M.; Born, S.; and Schmidt-Thieme, L. 2024. Physiome-ODE: A Benchmark for Irregularly Sampled Multivariate Time-Series Forecasting Based on Biological ODEs. In *The Thirteenth International Conference on Learning Representations*.
- Liu, J.; Cao, M.; and Chen, S. 2025. Timecheat: A Channel Harmony Strategy for Irregularly Sampled Multivariate Time Series Analysis. In *Proceedings of the AAAI Conference on Artificial Intelligence*, volume 39, 18861–18869.
- Liu, Y.; Hu, T.; Zhang, H.; Wu, H.; Wang, S.; Ma, L.; and Long, M. 2023. iTransformer: Inverted Transformers Are Effective for Time Series Forecasting. In *The Twelfth International Conference on Learning Representations*.
- Loshchilov, I.; and Hutter, F. 2019. Decoupled Weight Decay Regularization. arXiv:1711.05101.
- Menne, M. J.; Williams, J.; and Vose, R. S. 2006. U.S. HISTORICAL CLIMATOLOGY NETWORK (USHCN): Daily Temperature, Precipitation and Snow Data. Technical report, Environmental System Science Data Infrastructure for a Virtual Ecosystem (ESS-DIVE) (United States); Carbon Dioxide Information Analysis Center (CDIAC), Oak Ridge National Laboratory (ORNL), Oak Ridge, TN (United States).
- Nie, Y.; Nguyen, N. H.; Sinthong, P.; and Kalagnanam, J. 2022. A Time Series Is Worth 64 Words: Long-term Forecasting with Transformers. In *The Eleventh International Conference on Learning Representations*.
- Rubanova, Y.; Chen, R. T. Q.; and Duvenaud, D. K. 2019. Latent Ordinary Differential Equations for Irregularly-Sampled Time Series. In *Advances in Neural Information Processing Systems*, volume 32. Curran Associates, Inc.
- Schirmer, M.; Eltayeb, M.; Lessmann, S.; and Rudolph, M. 2022. Modeling Irregular Time Series with Continuous Recurrent Units. In *Proceedings of the 39th International Conference on Machine Learning, 19388–19405*. PMLR.
- Scholz, R.; Born, S.; Duong-Trung, N.; Cruz-Bournazou, M. N.; and Schmidt-Thieme, L. 2022. Latent Linear ODEs with Neural Kalman Filtering for Irregular Time Series Forecasting.
- Shukla, S. N.; and Marlin, B. 2020. Multi-Time Attention Networks for Irregularly Sampled Time Series. In *International Conference on Learning Representations*.
- Silva, I.; Moody, G.; Scott, D. J.; Celi, L. A.; and Mark, R. G. 2012. Predicting In-Hospital Mortality of ICU Patients: The PhysioNet/Computing in Cardiology Challenge 2012. In *2012 Computing in Cardiology*, 245–248.
- Tolstikhin, I. O.; Houlsby, N.; Kolesnikov, A.; Beyer, L.; Zhai, X.; Unterthiner, T.; Yung, J.; Steiner, A.; Keysers, D.; Uszkoreit, J.; Lucic, M.; and Dosovitskiy, A. 2021. MLP-Mixer: An All-MLP Architecture for Vision. In *Advances in Neural Information Processing Systems*, volume 34, 24261–24272. Curran Associates, Inc.
- Vaswani, A.; Shazeer, N.; Parmar, N.; Uszkoreit, J.; Jones, L.; Gomez, A. N.; ukasz Kaiser, Ł.; and Polosukhin, I. 2017. Attention Is All You Need. In *Advances in Neural Information Processing Systems*, volume 30. Curran Associates, Inc.
- Vedrana Vidulin, M. L. 2010. Localization Data for Person Activity.
- Wu, H.; Hu, T.; Liu, Y.; Zhou, H.; Wang, J.; and Long, M. 2022. TimesNet: Temporal 2D-Variation Modeling for General Time Series Analysis. In *The Eleventh International Conference on Learning Representations*.
- Wu, H.; Xu, J.; Wang, J.; and Long, M. 2021. Autoformer: Decomposition Transformers with Auto-Correlation for Long-Term Series Forecasting. In *Advances in Neural Information Processing Systems*, volume 34, 22419–22430. Curran Associates, Inc.
- Yalavarthi, V. K.; Burchert, J.; and Schmidt-Thieme, L. 2023. Tripletformer for Probabilistic Interpolation of Irregularly Sampled Time Series. In *2023 IEEE International Conference on Big Data (BigData)*, 986–995.

Yalavarthi, V. K.; Madhusudhanan, K.; Scholz, R.; Ahmed, N.; Burchert, J.; Jawed, S.; Born, S.; and Schmidt-Thieme, L. 2024a. GraFITi: Graphs for Forecasting Irregularly Sampled Time Series. *Proceedings of the AAAI Conference on Artificial Intelligence*, 38(15): 16255–16263.

Yalavarthi, V. K.; Scholz, R.; Born, S.; and Schmidt-Thieme, L. 2024b. Probabilistic Forecasting of Irregular Time Series via Conditional Flows. *CoRR*, abs/2402.06293.

Yalavarthi, V. K.; Scholz, R.; Madhusudhanan, K.; Born, S.; and Schmidt-Thieme, L. 2024c. Marginalization Consistent Mixture of Separable Flows for Probabilistic Irregular Time Series Forecasting. arXiv:2406.07246.

Zeng, A.; Chen, M.; Zhang, L.; and Xu, Q. 2023. Are Transformers Effective for Time Series Forecasting? *Proceedings of the AAAI Conference on Artificial Intelligence*, 37(9): 11121–11128.

Zhang, B.; and Sennrich, R. 2019. Root Mean Square Layer Normalization. In *Advances in Neural Information Processing Systems*, volume 32. Curran Associates, Inc.

Zhang, J.; Zheng, S.; Cao, W.; Bian, J.; and Li, J. 2023. Warpformer: A Multi-scale Modeling Approach for Irregular Clinical Time Series. In *Proceedings of the 29th ACM SIGKDD Conference on Knowledge Discovery and Data Mining*, KDD '23, 3273–3285. New York, NY, USA: Association for Computing Machinery. ISBN 9798400701030.

Zhang, W.; Yin, C.; Liu, H.; Zhou, X.; and Xiong, H. 2024a. Irregular Multivariate Time Series Forecasting: A Transformable Patching Graph Neural Networks Approach. In *Forty-First International Conference on Machine Learning*.

Zhang, W.; Zhang, L.; Han, J.; Liu, H.; Fu, Y.; Zhou, J.; Mei, Y.; and Xiong, H. 2024b. Irregular Traffic Time Series Forecasting Based on Asynchronous Spatio-Temporal Graph Convolutional Networks. In *Proceedings of the 30th ACM SIGKDD Conference on Knowledge Discovery and Data Mining*, 4302–4313. Barcelona Spain: ACM.

Zhang, X.; Zeman, M.; Tsiligkaridis, T.; and Zitnik, M. 2021. Graph-Guided Network for Irregularly Sampled Multivariate Time Series. In *International Conference on Learning Representations*.

Zhang, Y.; and Yan, J. 2022. Crossformer: Transformer Utilizing Cross-Dimension Dependency for Multivariate Time Series Forecasting. In *The Eleventh International Conference on Learning Representations*.

Zhou, H.; Zhang, S.; Peng, J.; Zhang, S.; Li, J.; Xiong, H.; and Zhang, W. 2021. Informer: Beyond Efficient Transformer for Long Sequence Time-Series Forecasting. *Proceedings of the AAAI Conference on Artificial Intelligence*, 35(12): 11106–11115.

Zhou, T.; Ma, Z.; Wen, Q.; Wang, X.; Sun, L.; and Jin, R. 2022. FEDformer: Frequency Enhanced Decomposed Transformer for Long-term Series Forecasting. In *Proceedings of the 39th International Conference on Machine Learning*, 27268–27286. PMLR.

A Datasets

PhysioNet (Silva et al. 2012) and **MIMIC** (Johnson et al. 2016) both contain the vital signs of intensive care unit patients. To evaluate the models, we query them to forecast all the measured variables for 24 hours based on all observations from the initial 24 hours after a patient’s admission.

Human Activity (Vedrana Vidulin 2010) contains 3-dimensional positional records of four sensors attached resulting in 12 variables. The sensors are attached to individuals who perform various activities (walking, sitting among others). Models are tasked with predicting 1 second of human motion based on 3 seconds of observation.

Finally, **USHCN** (Menne, Williams, and Vose 2006) is created by combining daily meteorological measurements from over one thousand weather stations that are distributed over the US. While the 3 datasets mentioned above contain sparsely sampled IMTS intrinsically, USHCN originally was observed regularly and transformed into IMTS by randomly sampling observations. In each IMTS we use 2 years of observations to predict the climate conditions of a single month. For each dataset we split the samples into 60% train 20% validation and 20% test data. Additional information about the datasets are given in Table 6. We calculate the Sparsity of each dataset by dividing the number of non-missing observations (N_{OBS}) by the number of given observation steps (N_T) times the number of channels (C): $\text{Sparsity} = \frac{N_{\text{OBS}}}{N_T C}$

Previous works (De Brouwer et al. 2019; Biloš et al. 2021; Schirmer et al. 2022; Yalavarthi et al. 2024a) used the parts of these datasets, but with different preprocessing, chunking and validation protocols. We want to emphasize that therefore, the results reported in these works are incomparable.

Table 6: Summary of dataset characteristics. *Obs. / Forc. Range* refers to the observation range and forecasting horizon. *Instances* are the IMTS from training- validation- and test set combined. *Channels* are the number of variables observed. *min/max avg. Obs.* refers to the minimum/maximum number of observation per channel averaged over instances.

	PhysioNet	MIMIC	H. Activity	USHCN
Obs. / Forc. range	24h/24h	24h/24h	3s/1s	2y/1m
Sparsity	86%	97%	75%	78%
Instances	12,000	23,457	5,400	26,736
Channels	41	96	12	5
min avg. Obs.	0.07	0.0007	19.7	32.7
max avg. Obs.	31.1	3.3	23.9	35.6

B Experimental Details

IMTS-Mixer For the PMAU benchmark, we sample 20 hyperparameter configurations and select the one with the lowest MSE on the validation split. For Physiome-ODE, we adhere to the proposed protocol and conduct random search with 10 configurations and evaluating them on the validation set of a single fold (Klöttergens et al. 2024). Furthermore, we set the hidden dimension of the non-linear networks that encode observation and query time stamps to

32. To train IMTS-Mixer, we implement the schedule-free AdamW (Kingma and Ba 2017; Loshchilov and Hutter 2019; Defazio et al. 2024) optimizer with an initial learning rate of 0.01 and use early stopping with patience of 20 epochs. We use a batch-size of 32.

- We tune the dimension of the aggregated channels D from the set $\{64, 128, 256\}$
- The range for D_{OUT} is $\{32, 64, 128\}$
- We allow the number of mixer blocks to be $\{1, 2, 3\}$
- We tune the weight decay from $\{1e-2, 1e-3, 1e-4\}$

GraFITi We refer to the hyperparameters as given in the GitHub repository from GraFITi (Yalavarthi et al. 2024a): <https://github.com/yalavarthivk/GraFITi>

- PhysioNet: 4 layers, 4 heads, latent-dimension of 64 and a batch size of 32
- MIMIC: 4 layers, 4 heads, latent-dimension of 64 and a batch size of 32
- Activity: 4 layers, 4 heads, latent-dimension of 64 and a batch size of 32
- USHCN: 2 layers, 2 heads, latent-dimension of 128 and a batch size of 32

To compare our model with GraFITi on the Physiome-ODE benchmark in terms of parameter count and inference term, we retain the hyperparameter parameters by following the search protocol as described in Klöttergens et al. (2024).

TimeCHEAT (Liu, Cao, and Chen 2025) We used the code as published in:

<https://github.com/Alrash/TimeCHEAT>. The batch-size is set to 32 and following the published implementation, we use a decay on plateau scheduler with Adam optimizer and an initial learning of 0.001. For TimeCHEAT we tuned the hyperparameters from the following grid:

- Number of transformer layers: $\{1, 2, 3\}$
- Transformer hidden dimension: $\{64, 128, 256\}$
- Number of encoder layers: $\{1, 2, 4\}$
- The initial learning rate is tuned from $\{1e-4, 1e-3\}$

TSMixer We use PyTorch implementation from TSMixer (Chen et al. 2023) as published here:

<https://github.com/ditschuk/pytorch-tsmixer>. TSMixer is applied as follows: Timestamps and a binary mask indicating whether a channel is observed at a given time step are used as additional variables, which are not forecasted. Query timestamps are input into the model as future covariates. The model is trained using the AdamW optimizer, with a weight decay of 0.0001 and a batch size of 32. We tune these following hyperparameters by random search from the these ranges:

- The initial learning rate is tuned from $\{1e-4, 1e-3\}$
- Dropout: $\{0.0, 0.1, 0.2\}$
- Number of Mixer Blocks: $\{1, 2, 3\}$

tPatchGNN For tPatchGNN (Zhang et al. 2024a), we use the implementation as published here: <https://github.com/usail-hkust/t-PatchGNN>

- The hidden dimension is selected from $\{32, 64, 128\}$
- The time embedding dimension is taken from $\{5, 10, 20\}$
- The initial learning rate is tuned from $\{1e-4, 1e-3\}$
- The patch size
 - is tuned from $\{2, 4, 8\}$ for PhysioNet, MIMIC, USHCN
 - is tuned from $\{100, 300, 750\}$ for Activity

C Physiome-ODE

We report the test MSE of GraFITi-C (Klöttergens et al. 2024), Neural Flows (Biloš et al. 2021), CRU (Schirmer et al. 2022), LinODENet (Scholz et al. 2022), GraFITi (Yalavarthi et al. 2024a), tPatchGNN (Zhang et al. 2024a), TimeCHEAT (Liu, Cao, and Chen 2025), and IMTS-Mixer on each dataset of the Physiome-ODE benchmark (Klöttergens et al. 2024) in Table 7.

The number of parameters from each model for each dataset is shown in Table 8.

Additionally, we list the respective inference times in Table 9. For all models, we use an NVIDIA 1080Ti and a batch size of 32.

D Multi-Head Attention for Irregular Channels

In Section 6.4, we discuss replacing ISCAM with a single multi-head attention (Vaswani et al. 2017)(MHA)-Block. Hence, we infer the hidden state of channel c with:

$$Z_c^{\text{MHA}} = \mathcal{H}_c + \text{ReLU}\left(\text{Linear}_{\text{MHA}}(\mathcal{H})\right), \quad \text{with}$$

$$\mathcal{H}_c = \text{MHA}\left(\mathcal{Q}_c, \mathcal{K}_c, \mathcal{V}_c\right)$$

To aggregate a channel into a fixed-sized vector, we use a singular query \mathcal{Q}_c that is implemented with a learnable channel representation. Following previous work (Yalavarthi et al. 2024a; Liu, Cao, and Chen 2025), we use the sequence of encoded time-value tuples as keys and values ($\mathcal{K}_c = \mathcal{V}_c$). Here, these tuples are encoded by concatenating the scalar value to a sinusoidal time-embedding.

In the hyperparameter tuning of this ablation study we additionally select the number of attention heads from $\{1, 2, 4, 8\}$.

Dataset	IMTS-Mixer	TimeCHEAT	tPatchGNN	GraFITi	LinODENet	CRU	Neural Flows	GraFITi-C
DUP01	<u>0.954± 0.038</u>	0.978± 0.030	0.957± 0.035	0.955± 0.037	0.964± 0.036	0.958± 0.038	1.030± 0.046	0.951± 0.036
JEL01	0.935± 0.018	0.966± 0.027	0.943± 0.016	0.942± 0.020	0.949± 0.015	0.939± 0.015	1.000± 0.013	0.935± 0.016
DOK01	0.978± 0.005	0.997± 0.004	0.987± 0.004	0.984± 0.005	0.996± 0.003	0.985± 0.005	0.998± 0.005	<u>0.982± 0.005</u>
INA01	1.003± 0.009	1.005± 0.010	<u>1.004± 0.009</u>	<u>1.004± 0.010</u>	1.009± 0.011	1.005± 0.010	1.008± 0.008	<u>1.004± 0.009</u>
WOL01	0.783± 0.026	0.804± 0.029	0.795± 0.027	0.787± 0.028	0.806± 0.027	0.814± 0.029	0.841± 0.029	<u>0.784± 0.030</u>
BOR01	0.708± 0.021	0.718± 0.022	0.719± 0.019	0.712± 0.022	0.719± 0.021	0.715± 0.020	0.743± 0.026	<u>0.709± 0.022</u>
HYN01	0.608± 0.048	0.652± 0.049	0.630± 0.045	0.625± 0.043	0.672± 0.044	0.665± 0.053	0.636± 0.045	<u>0.619± 0.046</u>
JEL02	0.664± 0.030	0.714± 0.027	0.702± 0.023	0.699± 0.029	0.693± 0.031	<u>0.674± 0.028</u>	0.779± 0.028	0.687± 0.027
DUP02	<u>0.719± 0.046</u>	0.748± 0.047	0.728± 0.049	0.728± 0.044	0.740± 0.042	<u>0.722± 0.046</u>	0.890± 0.081	0.718± 0.046
WOL02	0.640± 0.014	0.679± 0.012	0.656± 0.016	0.654± 0.014	0.663± 0.015	0.653± 0.017	0.685± 0.012	<u>0.645± 0.016</u>
DIF01	<u>0.959± 0.029</u>	0.977± 0.031	0.991± 0.027	0.985± 0.030	0.832± 0.087	0.985± 0.025	1.014± 0.025	0.982± 0.029
VAN01	0.240± 0.005	0.252± 0.007	0.247± 0.007	0.246± 0.005	0.250± 0.006	0.253± 0.005	0.250± 0.006	<u>0.242± 0.006</u>
DUP03	0.610± 0.050	0.683± 0.046	0.624± 0.052	0.627± 0.043	0.632± 0.044	<u>0.622± 0.047</u>	1.098± 0.447	0.744± 0.042
BER01	0.277± 0.013	0.311± 0.028	0.310± 0.014	0.300± 0.018	<u>0.279± 0.020</u>	0.280± 0.016	0.398± 0.014	0.342± 0.018
LEN01	<u>0.547± 0.043</u>	0.932± 0.112	0.981± 0.062	0.607± 0.055	0.387± 0.071	0.754± 0.157	1.009± 0.061	0.970± 0.063
LI01	<u>0.177± 0.018</u>	0.438± 0.019	0.394± 0.028	0.202± 0.013	0.084± 0.009	<u>0.175± 0.020</u>	0.979± 0.049	0.742± 0.010
LI02	0.360± 0.047	0.464± 0.048	0.438± 0.048	<u>0.397± 0.058</u>	0.434± 0.044	0.437± 0.046	0.674± 0.105	0.458± 0.056
REV01	0.603± 0.045	0.741± 0.057	0.741± 0.054	0.674± 0.055	0.597± 0.061	<u>0.602± 0.049</u>	0.978± 0.042	0.855± 0.050
PUR01	<u>0.143± 0.017</u>	0.343± 0.017	0.397± 0.082	0.153± 0.006	0.106± 0.006	0.353± 0.083	0.654± 0.102	0.476± 0.020
NYG01	0.237± 0.051	0.402± 0.061	0.357± 0.067	<u>0.344± 0.065</u>	0.358± 0.071	0.403± 0.092	0.442± 0.094	0.366± 0.047
PUR02	0.251± 0.022	0.474± 0.057	0.390± 0.017	0.322± 0.021	<u>0.280± 0.028</u>	0.293± 0.026	0.723± 0.077	0.511± 0.023
HOD01	0.383± 0.052	0.511± 0.043	0.479± 0.057	0.493± 0.046	0.441± 0.043	<u>0.409± 0.049</u>	0.701± 0.077	0.609± 0.056
REE01	0.031± 0.005	0.044± 0.007	0.047± 0.011	<u>0.033± 0.007</u>	0.045± 0.012	<u>0.051± 0.008</u>	0.045± 0.011	0.039± 0.012
VIL01	0.302± 0.038	0.385± 0.045	0.354± 0.028	<u>0.344± 0.044</u>	0.374± 0.021	0.373± 0.039	0.500± 0.060	0.378± 0.042
KAR01	0.033± 0.012	0.050± 0.013	0.048± 0.012	0.041± 0.013	<u>0.034± 0.008</u>	0.044± 0.012	0.069± 0.009	0.078± 0.011
SHO01	0.053± 0.007	0.085± 0.019	0.078± 0.012	0.062± 0.013	0.057± 0.006	0.095± 0.010	0.092± 0.014	<u>0.055± 0.013</u>
BUT01	0.180± 0.036	0.306± 0.079	0.354± 0.102	0.281± 0.071	<u>0.254± 0.074</u>	0.317± 0.108	0.441± 0.153	0.324± 0.091
MAL01	0.014± 0.004	0.044± 0.002	0.038± 0.011	0.020± 0.004	<u>0.018± 0.007</u>	0.064± 0.007	0.052± 0.002	0.054± 0.005
ASL01	0.013± 0.004	0.029± 0.003	0.031± 0.004	0.025± 0.009	<u>0.022± 0.003</u>	0.046± 0.014	0.066± 0.033	0.026± 0.002
BUT02	0.156± 0.022	0.272± 0.031	0.280± 0.043	0.248± 0.052	<u>0.207± 0.056</u>	0.282± 0.042	0.329± 0.068	0.256± 0.039
MIT01	0.003± 0.000	0.008± 0.004	0.003± 0.000					
GUP01	0.011± 0.004	0.060± 0.014	0.047± 0.016	0.041± 0.006	<u>0.018± 0.007</u>	0.057± 0.017	0.043± 0.017	0.035± 0.006
GUY01	0.004± 0.001	0.015± 0.004	0.005± 0.001	0.005± 0.003	0.006± 0.005	0.004± 0.001	0.024± 0.015	0.004± 0.001
PHI01	0.105± 0.022	0.308± 0.019	0.249± 0.032	0.222± 0.013	<u>0.131± 0.014</u>	0.133± 0.020	0.635± 0.158	0.345± 0.015
GUY02	0.007± 0.002	0.032± 0.006	0.016± 0.003	0.012± 0.009	<u>0.010± 0.006</u>	<u>0.010± 0.002</u>	0.082± 0.066	0.032± 0.015
PUL01	0.006± 0.002	0.036± 0.011	0.018± 0.006	<u>0.008± 0.001</u>	<u>0.008± 0.004</u>	0.012± 0.003	0.061± 0.060	0.024± 0.008
CAL01	0.074± 0.005	0.720± 0.357	0.212± 0.033	0.179± 0.012	<u>0.078± 0.009</u>	0.158± 0.008	0.867± 0.014	0.643± 0.024
WOD01	0.098± 0.007	0.372± 0.293	0.165± 0.012	0.164± 0.013	0.154± 0.016	<u>0.113± 0.017</u>	0.510± 0.060	0.344± 0.016
GUP02	0.397± 0.016	0.445± 0.018	0.463± 0.024	0.449± 0.027	0.469± 0.022	<u>0.444± 0.018</u>	0.577± 0.017	0.461± 0.025
M01	0.003± 0.000	0.013± 0.002	0.004± 0.001	0.003± 0.000	0.004± 0.001	0.005± 0.000	0.124± 0.207	0.003± 0.000
LEN02	0.031± 0.005	0.217± 0.108	0.089± 0.011	0.099± 0.021	<u>0.039± 0.005</u>	0.059± 0.012	0.380± 0.141	0.143± 0.022
KAR02	<u>0.143± 0.007</u>	0.196± 0.008	0.160± 0.009	0.151± 0.009	0.140± 0.010	0.151± 0.011	0.257± 0.016	0.252± 0.010
SHO02	0.021± 0.003	0.063± 0.015	0.070± 0.017	0.043± 0.006	<u>0.037± 0.006</u>	0.083± 0.015	0.109± 0.015	0.073± 0.010
MAC01	0.016± 0.002	0.046± 0.005	0.033± 0.003	0.021± 0.003	0.020± 0.003	0.065± 0.006	0.029± 0.011	<u>0.019± 0.002</u>
IRI01	0.027± 0.005	0.053± 0.011	0.048± 0.008	0.038± 0.017	<u>0.037± 0.003</u>	0.049± 0.010	0.116± 0.006	0.097± 0.008
BAG01	0.026± 0.002	0.050± 0.003	0.045± 0.003	<u>0.029± 0.002</u>	<u>0.032± 0.005</u>	0.046± 0.005	0.075± 0.012	0.109± 0.002
WOL03	0.062± 0.009	0.233± 0.053	0.142± 0.024	<u>0.105± 0.016</u>	<u>0.073± 0.010</u>	0.177± 0.016	0.479± 0.107	0.247± 0.032
WAN01	0.082± 0.007	0.170± 0.014	0.140± 0.011	0.119± 0.010	<u>0.103± 0.012</u>	0.125± 0.012	0.345± 0.027	0.232± 0.015
NEL01	0.006± 0.001	0.019± 0.001	0.013± 0.001	<u>0.007± 0.000</u>	0.010± 0.001	0.009± 0.001	0.060± 0.029	0.023± 0.006
HUA01	0.037± 0.001	0.099± 0.006	0.090± 0.012	0.063± 0.005	<u>0.052± 0.004</u>	0.116± 0.007	0.149± 0.015	0.115± 0.007

Table 7: Test MSE on the Physiome-ODE (Klöttergens et al. 2024) benchmark. The results for the competing models are reported from the Physiome-ODE paper.

Dataset	IMTS-Mixer	TimeCHEAT	tPatchGNN	GraFITi
DUP01	173,075	1,279,382	365,594	315,329
JEL01	39,053	1,279,382	390,170	236,673
DOK01	105,219	338,203	159,610	1,255,297
INA01	139,891	337,282	159,830	15,825
WOL01	95,195	344,723	390,310	315,777
BOR01	178,201	341,702	365,614	1,253,377
HYN01	315,631	339,608	365,994	1,255,809
JEL02	17,741	645,014	365,594	627,329
DUP02	42,317	341,702	165,454	627,457
WOL02	192,745	343,695	160,414	315,649
DIF01	52,321	659,850	159,570	1,255,041
VAN01	80,459	642,011	390,330	1,254,273
DUP03	56,083	653,849	365,594	158,017
BER01	95,625	641,920	365,774	1,254,401
LEN01	42,317	646,214	365,614	315,393
LI01	65,179	343,376	365,654	315,521
LI02	48,095	343,376	365,654	1,253,633
REV01	44,699	1,282,256	390,230	1,253,633
PUR01	59,109	341,702	165,454	315,393
NYG01	139,891	343,747	165,974	1,256,705
PUR02	65,165	646,214	165,454	1,253,377
HOD01	62,141	342,531	390,210	1,253,505
REE01	39,997	655,491	365,634	315,457
VIL01	236,175	334,849	165,574	315,777
KAR01	130,321	644,156	390,450	1,255,041
SHO01	700,145	679,820	166,514	1,260,161
BUT01	61,353	342,531	390,210	1,253,505
MAL01	236,725	344,336	165,574	315,777
ASL01	143,079	651,229	390,730	1,256,833
BUT02	62,141	342,531	390,210	1,253,505
MIT01	192,745	344,082	165,534	236,993
GUP01	39,997	332,915	165,474	1,253,505
GUY01	168,461	340,631	165,434	5,249
PHI01	199,845	1,280,582	159,310	1,253,377
GUY02	168,461	653,462	390,170	236,673
PUL01	168,461	653,462	159,290	158,017
CAL01	284,951	1,282,977	390,470	1,255,169
WOD01	56,473	638,710	165,454	1,253,377
GUP02	45,205	655,491	159,330	1,253,505
M01	193,811	340,502	365,594	158,017
LEN02	176,997	638,710	159,310	1,253,377
KAR02	115,255	335,936	390,390	1,254,657
SHO02	528,233	672,187	166,514	1,260,161
MAC01	52,913	343,953	390,270	315,649
IRI01	97,937	654,482	390,590	316,673
BAG01	85,813	657,425	365,734	628,225
WOL03	275,821	658,641	365,814	1,254,657
WAN01	44,699	640,642	159,350	1,253,633
NEL01	62,141	342,789	365,634	1,253,505
HUA01	130,093	348,077	365,914	1,255,297

Table 8: Exact number of trainable parameters on each Physiome-ODE dataset.

Dataset	IMTS-Mixer	TimeCHEAT	tPatchGNN	GraFITi
DUP01	0.064	2.772	0.088	1.508
JEL01	0.061	2.704	0.125	1.419
DOK01	0.078	2.377	0.117	1.596
INA01	0.087	2.511	0.136	1.503
WOL01	0.063	2.461	0.153	1.517
BOR01	0.059	2.509	0.095	1.504
HYN01	0.092	2.526	0.154	1.601
JEL02	0.058	2.617	0.090	1.343
DUP02	0.053	2.398	0.113	1.342
WOL02	0.066	2.520	0.110	1.482
DIF01	0.071	2.623	0.107	1.592
VAN01	0.063	2.360	0.148	1.404
DUP03	0.056	2.316	0.089	1.201
BER01	0.065	2.450	0.128	1.473
LEN01	0.054	2.555	0.093	1.482
LI01	0.064	2.383	0.103	1.504
LI02	0.058	2.484	0.100	1.514
REV01	0.061	2.708	0.129	1.505
PUR01	0.060	2.530	0.122	1.531
NYG01	0.097	2.479	0.222	1.598
PUR02	0.054	2.575	0.101	1.500
HOD01	0.061	2.500	0.129	1.530
REE01	0.062	2.640	0.096	1.505
VIL01	0.070	2.375	0.164	1.508
KAR01	0.073	2.484	0.224	1.536
SHO01	0.115	2.724	0.359	1.604
BUT01	0.058	2.376	0.117	1.493
MAL01	0.066	2.445	0.146	1.484
ASL01	0.076	2.313	0.300	1.387
BUT02	0.062	2.523	0.122	1.506
MIT01	0.062	2.344	0.126	1.290
GUP01	0.056	2.284	0.118	1.390
GUY01	0.063	2.432	0.116	1.265
PHI01	0.061	2.808	0.091	1.509
GUY02	0.060	2.599	0.121	1.442
PUL01	0.060	2.576	0.089	1.356
CAL01	0.075	2.537	0.213	1.462
WOD01	0.059	2.581	0.107	1.527
GUP02	0.055	2.644	0.089	1.502
M01	0.064	2.538	0.098	1.364
LEN02	0.061	2.566	0.095	1.523
KAR02	0.065	2.479	0.242	1.503
SHO02	0.141	3.060	0.286	1.711
MAC01	0.061	2.379	0.161	1.510
IRI01	0.072	2.504	0.197	1.482
BAG01	0.057	2.368	0.113	1.260
WOL03	0.068	2.498	0.137	1.483
WAN01	0.063	2.521	0.100	1.501
NEL01	0.056	2.315	0.093	1.366
HUA01	0.075	2.514	0.137	1.568

Table 9: Inference time in seconds of each model on the datasets contained in the Physiome-ODE benchmark.